Optical networks as complex lasers

Giovanni Giacomelli,[1] Stefano Lepri,[1] and Cosimo Trono[2]
[1]*Consiglio Nazionale delle Ricerche, Istituto dei Sistemi Complessi, Via Madonna del Piano 10 I-50019 Sesto Fiorentino, Italy*
[2]*Consiglio Nazionale delle Ricerche, Istituto di Fisica Applicata "Nello Carrara," Via Madonna del Piano 10 I-50019 Sesto Fiorentino, Italy*

(Received 1 August 2018; published 22 February 2019)

We discuss the main features of a recently introduced system capable of laser action: the complex active optical network, or lasing network (LANER) [Lepri *et al.*, Phys. Rev. Lett. **118**, 123901 (2017)]. The system is experimentally realized with optical fibers linked each other with couplers and with one or more coherently amplifying sections. The LANER displays a standard laser behavior: When the gain provided by the active sections is high enough to overcome the losses, a coherent emission is produced, with a complicated intensity spectrum. A linear theoretical description is discussed in detail, showing how the LANER can be considered as a generalization of the laser with the physical network acting as a complicated cavity. Among its main aspects, the system can be represented by directed graphs disclosing the analogies with the problem of quantum chaos on graphs. Moreover, when the links' lengths are all integer multiples of the same value, the LANER framework corresponds to a lattice problem, with the equivalence of the Brillouin zone with the cavity free spectral range. Experiments in simple configurations are also performed, reporting the evidence of lasing action and its characterization. Examples of spectra of the detected emitted intensity are obtained in different cases, in a phenomenological agreement with the numerical findings of the theory.

DOI: 10.1103/PhysRevA.99.023841

I. INTRODUCTION

The concepts of networks and graphs are central in complexity science. Countless examples of systems where irregular connectivity of agents plays a central role in the dynamics and emergent properties are discussed in the scientific literature [1]. In view of the many possible natural realizations in physics, biology, and even social sciences, the study of nonlinear dynamical systems on graphs is *per se* a relevant research topic [2]. Just to mention a few examples, this is relevant for the functioning of power grids and their failures [3] and the roles of topology in synchronization [4], spatial [5] and quantum [6,7] networks, and other nonlinear effects [8,9]. Dynamics of nonlinear fields on graphs, for instance, starlike structures, has also attracted the interest of theoreticians [10,11]. However, most of the above topics could be quite difficult to study in real systems and even more so in controlled laboratory conditions.

Laser systems have been historically used as test beds for many ideas from nonlinear dynamics and statistical or condensed-matter physics and could represent suitable candidates for such an investigation. On the other hand, since the very first proposals, the great majority of lasers have shared the same structure: a gain section in a simple linear or ring cavity, supporting regular sets of optical modes [12]. The opposite case is represented by the random laser, where the propagation of rays in a disordered gain medium leads to light amplification [13,14]. In fact, both such frameworks are inadequate to provide the richness and the complexity required for a characterization of specific statistical and/or dynamical issues in the network theory. The recently introduced Lasing Network (LANER) [15] represents a system where the above difficulties can be overcome. In brief, it consists of an active optical network, whose connectivity induces a form of topological disorder and can display genuine laser action; indeed, the LANER could also be considered as a discrete random laser, with a controllable complexity [15]. The system permits scaling of the more standard laser geometries, embodied in the simpler configurations with a single gain, to strongly connected, multiple-gain setups. Moreover, from an experimental point of view, the apparatus has several practical advantages: Its flexibility allows exploration of different configurations by an easy rearrangement of the components. The stability of the setup grants detailed statistical analysis as well.

With respect to Ref. [15], here we first detail the theoretical description of the LANER and its relevant features. In particular, we discuss the properties of the matrices involved in the derivation of the modes and analyze the physical features of some limit cases. Simple configurations are investigated as examples. Then, an experimental realization is presented of the same setups, and we report evidence of the lasing action and the phenomenology of the power spectrum of the emitted intensity.

The plan of the paper is as follows. In Sec. II, we introduce the general idea and the main physical ingredients. A theoretical linear model to compute the modes via the network matrix of the LANER is presented in Sec. III. Some specific examples are illustrated in Sec. IV, where we also report a calculation of the optical spectra based on rational approximations of the lengths (Sec. V). The final part of the paper (Secs. VI A and VI B) is devoted to the description of the experimental realizations we have carried out and a summary of their phenomenology.

II. THE LANER CONCEPT

A sketch of the concept is depicted in Fig. 1. A physical network is built using single-mode optical fibers connected via

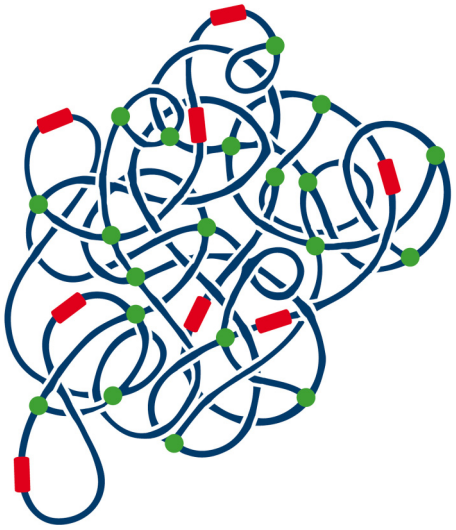

FIG. 1. The LANER concept. A physical network, built with optical fibers (blue) connected though standard components such as power splitters (green dots), acts as a laser with a complex cavity. The coherent gains are provided by active regions (red thick segments), employing, e.g., Er-doped fibers, semiconductor amplifiers, etc.

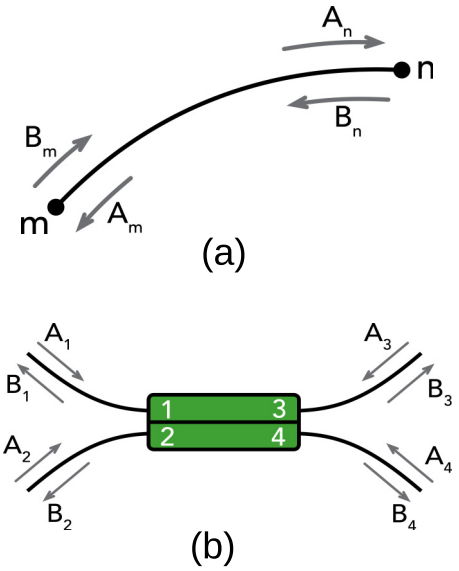

FIG. 2. The observables: the propagating fields at the extrema of the links (a) and at the ports of the splitters (b). The indexing shown is chosen only to distinguish each component of the fields for the two cases; in the general approach, a further index for the links and the splitters will be required.

standard optical components such as $m \times n$ power splitters, circulators, etc. Coherent gain sections, using the mechanism of stimulated emission are placed in one or more (active) links: laser-pumped, erbium-doped fibers, and/or semiconductor amplifiers or other systems can be used at this purpose. Alternative components can be employed to introduce or remove particular constraints in the structure; for instance, in the experiments described in this work, we will only deal with directed gains, realized by inserting optical isolators in the active links. The observable quantities are the emitted fields in the links, detected inserting (e.g., 2×2) power splitters (possibly with a small coupling ratio): The two propagation directions can be monitored at the same time if desired. The split fields can be thus sent to detection sections, where high bandwidth and sensitivity detectors monitor the field intensity.

III. THEORETICAL DESCRIPTION

For the theoretical description, we denote by L_j the length of the link j, spanning the N_l available fiber segments; in the present work, we consider the case in which all the ports of each splitter are connected to fibers so that $N_l = 2N_s$ and N_s is the number of 2×2 splitters. We consider the propagation delays through the splitters by a suitable redefinition of the L_j's. The main basic quantity we will deal with is the optical spectrum of stationary modes. Its calculation is based on a standard linear propagation approach and will be discussed in the following subsections.

A. The observables: The field in the links

We consider the electric field propagating in the link j

$$\mathbf{E}_j(t, \mathbf{r}_j) = \mathbf{E}_j^{(+)}(t, \mathbf{r}_j) + \mathbf{E}_j^{(-)}(t, \mathbf{r}_j), \tag{1}$$

in terms of the forward- and backward-propagating fields

$$\mathbf{E}_j^{(\pm)}(t, \mathbf{r}_j) = \mathbf{e}_y \Phi(\rho, \theta) f_j^{(\pm)}(t, z_j)\,. \tag{2}$$

Here, $\mathbf{r}_j = (\rho, \theta, z_j)$ is the cylindrical-coordinate vector in the link j, $\mathbf{e}_y$ is the unit vector indicating the linear (transverse) polarization directions, and Φ is the transverse mode profile, assumed to be the same for all the fibers. In single-mode fibers like those we have employed in the experiments, only the fundamental mode LP_{01}, which is a function of the radial coordinate ρ only is supported. The functions $f^{(\pm)}(t, z_j)$ describe the amplitude of the field propagating in the two directions at the point z_j of the j-link coordinate system.

In the present approach, we will consider that all the fields in the links of the physical network share the same polarization direction. While this can be experimentally realized by using polarization-maintaining fibers and components, the effect of possible different polarization directions in some links can be taken in account by a suitable redefinition of the corresponding gains. This approach is made possible by the fact that such effects would be fixed for a given experimental configuration.

The physical description of the LANER behavior is then carried out in terms of the propagating fields in each link. In particular, for a given link, we call A (respectively, B) the values of the field at the extremities exiting (respectively, entering) the link as shown in Fig. 2(a).

B. Connecting the links: The scattering matrix

We consider first a single 2×2 lossless coupler depicted in Fig. 2(b). We define, at each of the four ports, the column vectors of input and output amplitudes $A = (A_1, A_2, A_3, A_4)^T$ and $B = (B_1, B_2, B_3, B_4)^T$ (this requires fixing a port numbering). They are related via the scattering matrix $B = S^{(1)}A$. The splitting of the field follows an unitary transformation (energy conservation through the splitter). Under a prescribed convention, we can parameterize it through the transmission

and reflection coefficients T, R such that $|T| = \sqrt{\alpha}$ and $|R| = \sqrt{1-\alpha}$, where $0 \leqslant \alpha \leqslant 1$ is also termed as the splitting factor. Moreover, the splitters are reflectionless and this impose some further constraint on the form $S^{(1)}$. Altogether,

$$S^{(1)} = \begin{pmatrix} 0 & 0 & \sqrt{1-\alpha} & \sqrt{\alpha} \\ 0 & 0 & -\sqrt{\alpha} & \sqrt{1-\alpha} \\ \sqrt{1-\alpha} & -\sqrt{\alpha} & 0 & 0 \\ \sqrt{\alpha} & \sqrt{1-\alpha} & 0 & 0 \end{pmatrix}. \quad (3)$$

The blocks connecting $\{A_1, A_2\}$ with $\{B_3, B_4\}$ and $\{A_3, A_4\}$ with $\{B_1, B_2\}$ (upper right and bottom left respectively) are unitary matrix as noted before. As a consequence, the matrix $S^{(1)}$ is unitary as well.

In the case of N_s splitters that, for simplicity, we assume to be all equal as above, we can extend the definitions introducing the $4N_s$-dimensional column vectors of input and output amplitudes A and B whose components are taken ordered in such a way that

$$B = SA \quad (4)$$

and the complete $(4N_s \times 4N_s)$ scattering matrix is block-diagonal

$$S = \begin{pmatrix} S^{(1)} & 0 & \cdots & 0 \\ 0 & S^{(1)} & \cdots & 0 \\ \vdots & \vdots & \ddots & \vdots \\ 0 & 0 & \cdots & S^{(1)} \end{pmatrix}.$$

The unitary (orthogonal) matrix S describes the transfer properties of the splitters (or, in general, of the optical components at the physical nodes of the LANER) and is thus independent of the gains and the topology of the physical network. It is readily generalized to the case of a set of different splitters each having different transmission coefficients and/or port numbers.

It is worth noting that splitters may have rather different designs, translating into corresponding properties of S, such as (see, e.g., Ref. [16]) the following:

(i) *lossless* (S is unitary);

(ii) *reciprocal* (S is symmetric); and

(iii) *matched* (diagonal elements of S are zero).

In the present work, we will focus on the case of all equal 2×2, 50% power optical splitters, such that $\alpha = \frac{1}{2}$ which satisfies (i), (ii), and (iii).

C. Evolution in the links: The propagation matrix

In a linear description, we assume that the propagation of the field in the link j is described by gain $G_j = g_j e^{-(\mu+ik)L_j} = g_j e^{-sL_j}$, where $g_j > 1$ (respectively, < 1) represents real and positive link gain (respectively, losses), s is the complex wave vector, and L_j is the (oriented) link length. We note that the gains are written in the space domain: In the time domain, we would instead use the time delays L_j/v, where v is the light velocity in the fibers. In this way, the field at the end of the link is obtained by that at the beginning (along the propagation direction) by multiplying the latter by the gain. According to the definition of the field variables and introducing the $(2N_l \times 2N_l)$ propagation matrix P, we write

$$A = PB\,. \quad (5)$$

In a specific realization of the LANER, additional (fixed) link-coupler phase delays should be considered depending on the type of components. Such delays could be included in a more general form of the gains as

$$G_j^{(\pm)} \to G_j^{(\pm)} e^{i\phi_j^{(\pm)}}, \quad (6)$$

where the $(\pm)$ refers to the (chosen) propagation direction along the link, notably, $\phi_j^{(+)} = -\phi_j^{(-)}$. Associating the global phase delays to the elements of P allows us to write the matrix S in its simplest form; i.e., possible phase delays due to the couplers are now included in the propagation and not in the scattering matrix.

The matrix P contains both the topology (how the splitters connect the links) and metric (gain and links length) information of the LANER. As shown in Fig. 2(a), variables $\{A, B\}$ in the same link are related according to

$$A_n = g_j^{(+)} e^{-(\mu+ik)L_j} B_m = G_j^{(+)} B_m, \quad (7)$$

$$A_m = g_j^{(-)} e^{-(\mu-ik)L_j} B_n = G_j^{(-)} B_n, \quad (8)$$

where $j = j(n, m)$ is a (given) function of the splitter ports indexes numbering the links.

The matrix P has the following properties:

(1) Since every port of each splitter is connected to one and only one (different) port, P has only one nonvanishing entry in every row and in every column.

(2) Since the output of a port cannot be connected to itself, the diagonal elements of P are zero.

(3) It is invertible since

$$\det P = |G_1|^2 \times \cdots \times |G_{N_l}|^2$$
$$= (g_1^{(+)} g_1^{(-)}) \times \cdots \times (g_{N_l}^{(+)} g_{N_l}^{(-)}) \times \exp(-2\mu L) \neq 0,$$

where we have introduced the total length $L = L_1 + \cdots + L_{N_l}$.

In the particular case of symmetric gains $g_j^{(+)} = (g_j^{(-)})^*$ (i.e., $|g_j^{(+)}| = |g_j^{(-)}|$ since $\phi_j^{(+)} = -\phi_j^{(-)}$ as said) for every j, P is Hermitian (i.e., $P = P^\dagger$).

We will consider the case $\phi = 0$ for each link, since in our experiments phase delays are not present either in the fibers or in the power splitters. In such a case, $g_j^{(+)} = g_j^{(-)} = g_j$ and

$$P_{nm} = g_j e^{-sL_j} = G_j,\ P_{mn} = G_j^*. \quad (9)$$

Directed active gains, that we are using in the experiment reported here, correspond to set the blocked direction in the symmetric elements of P to zero. Notably, this is a strong source of losses, as the field incoming in the blocked direction is dissipated in the optical isolator.

D. The LANER matrix

The field stationary solution A can be obtained by setting

$$A = PB = PSA\,. \quad (10)$$

Equation (10) is satisfied for $A \neq 0$ if A is an eigenvector of the LANER matrix

$$N = PS, \quad (11)$$

with a corresponding eigenvalue $\lambda = 1$, leading to the characteristic equation[1]

$$\det(N - I) = 0, \tag{12}$$

where I is the identity matrix. The roots $\{s\}$ in the complex plane of the above equation can be found numerically by standard routines. Equation (12) allows for the complete determination both of the optical modes supported by the cavity (matching conditions for the field) and of the threshold condition (balance between the gains and the losses) in order to have them lasing. Analytic solutions of (12) are often very difficult to be found except for some simple cases.

We remark how, since the direction in every link is chosen arbitrarily, Eq. (12) must admit the same set of solutions for all the possible permutations $G_j^{(+)} \to G_j^{(-)}$ ($G_j \to G_j^*$ in the case of symmetric scalar gains), for $j \in H$ where H is an arbitrary subset of the links index set. H thus represents the subset of links where the propagation directions has been reverted.

Depending on the configuration (e.g., the topology of the connections), we expect that the corresponding matrix N might exhibit particular structures allowing the determination of the properties of the modes. This problem represents the mayor challenge of the linear, theoretical description of a LANER.

E. Lossless LANER (empty cavity limit): The Hamiltonian case

Let us now discuss two particular cases, starting with the situation of LANER with no gain nor losses, i.e., $g_j = 1$. This corresponds to the so-called empty cavity limit and can be described mathematically by setting the elements of the propagation matrix to pure dephasing terms only: $G_j \to e^{iKL_j}$ (with K real). The propagation matrix is thus unitary $P^\dagger = P$, reflecting the time-reversal invariance of the dynamics (which is obviously broken in the presence of gain and losses). As a consequence, the LANER matrix is unitary as well, $N^\dagger N = NN^\dagger = I$ and all the mode solutions of Eq. (12) are marginally stable (i.e., the real part of the poles are all zeros) and the dynamics would be akin to the one of a conservative system. In this case, all the possible modes can lase and the equation provides a way for calculating all of them regardless of their effective action in the dynamics.

We also remark the close analogies of this situation with quantum graphs which have been thoroughly investigated in the realm of quantum chaos [17–19]. In this context, N is termed the vertex scattering matrix. The equation for the poles, Eq. (12), is formally equal to the one to determine the quantum spectrum of a particle moving freely along the bonds and scattered at the graph vertices. As an interesting extension that may be of some relevance also in our case, we mention that a form of dissipation has been also studied by considering open graphs [19,20].

An experimental realization of quantum graphs is provided by microwave networks which have been investigated in recent years [21]. However, the LANER is not only different for being an optical system but also for having as a novel element the optical gain (possibly in multiple links) which allows us to achieve the lasing action.

From the general point of view of graph theory, a full description of the LANER will require solving the electromagnetic wave equation coupled with suitable equation(s) for population dynamics on the bonds. This would represent a more general (and complicated) framework with respect to the above discussed quantum graph limit. Of course, a suitable mapping procedure of the physical network to a graph will be required as well; in the next section, we indicate a possible approach to introduce a graph representation of the LANER.

F. LANER and graphs

Another interesting limit is the one in which the propagation approaches a "classical" limit corresponding to ray dynamics [22]. This point of view has been successfully employed to justify theoretically the Lévy distribution of emission fluctuations, akin to the one observed for random lasers [23–25]. To this aim, a Monte Carlo type of model has been simulated in Ref. [15]. It consists of two steps: (i) a free propagation of an ensemble of "rays" on the physical network, each having an intensity that grows or decreases depending on the local value of the gains g_j, and (ii) random transitions at each splitter with probabilities assigned according to the values of the splitting factors (see Ref. [15] for details).

In this situation, it should be also useful to introduce a simplified description of the dynamics as a (random) motion on a graph that can be introduced as follows. Each vertex of the graph represents a component of the field in a link and a directed bond is the linear dependence of the target on the source field. We define such a graph through its adjacency matrix obtained by setting all the nonzero elements of the matrix N to 1.

To illustrate the concept, we refer to the specific example with $N_l = 2N_s = 6$ sketched in Fig. 3(a). The numbers $1_\pm, 2_\pm, \ldots, 6_\pm$ denote the 12 field components propagating on each fiber and label the nodes of the associated graph, Fig. 3(b). This example leads to a regular directed graph as the number of incoming and outcoming links is equal to 2 for each vertex. A red vertex indicates that the related mode link is active; otherwise, it is passive if black. To illustrate how the connectivity can be changed, we show in Fig. 3(c) how the inclusion of isolators in the active links [represented in Fig. 3(a) by the red arrows indicating the allowed directions] leads to the removal of the blocked fields and therefore the corresponding vertices are removed from the graph, which is therefore pruned. It is worth noting that the system can lase only if at least one active vertex is present in the pruned graph.

At the simplest level of description, the ray dynamics in the LANER can be visualized as complicated motion yielding a Markovian random walk [26] on such graphs while amplification and damping can be introduced [15].

IV. LANER EXAMPLES

As examples, we discuss the simpler configurations realized with few splitters in the 50 : 50 splitting ratio case, i.e., $\alpha = 1/2$ in Eq. (3) and symmetric scalar gains. We notice how

[1]Equation (10) can be written in terms of B as well, using the matrix $M = SP$. In particular, the eigenvalues of N and M are the same.

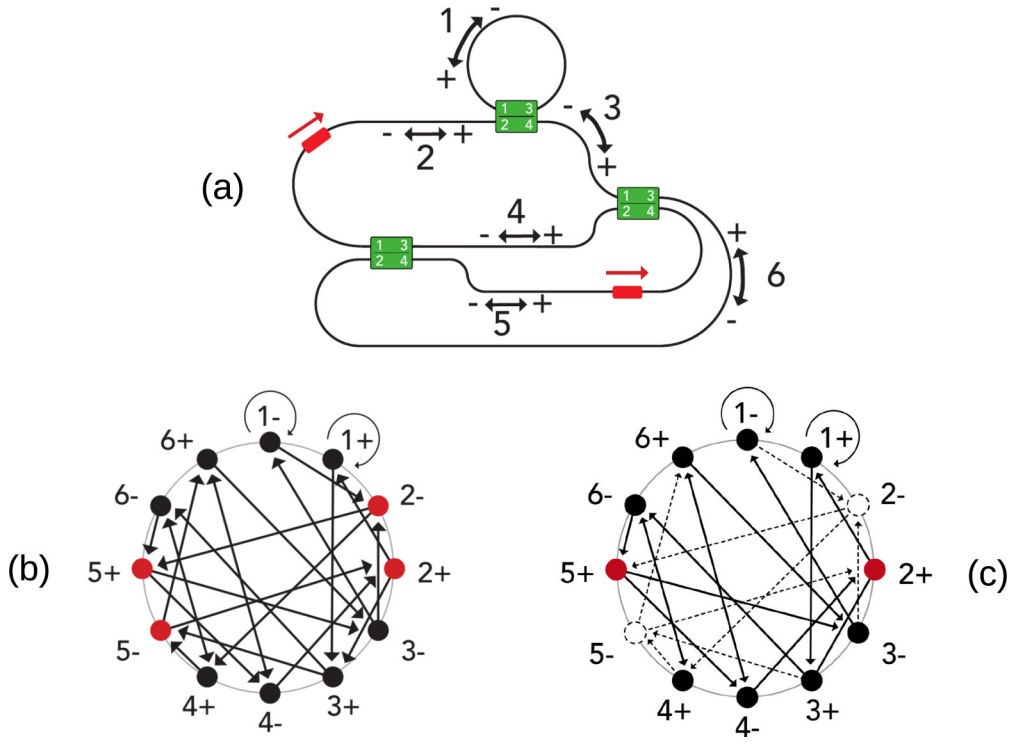

FIG. 3. A possible LANER configuration and its correspondent directed graph as described in the text. (a) The physical network: the thick, red segments indicate the gain sections and the black, numbered arrows are the propagating fields along the fiber links. The insertion of isolators imposes a single propagation direction in the active links (indicated by the red arrows on top of the gain sections). [(b), (c)] The graphs represent the fields as vertices and the connections induced by the splitters as bonds: A targeted mode is linearly dependent on the sourced one. The red and black dots indicate that the links are respectively active or passive. (c) Change in the connectivity induced by the insertion of the isolators in the physical network (a): The graph (b) is pruned as the opaque parts are removed.

the zero splitter LANER is the standard laser, either in a loop (ring) or linear cavity.

Starting with the case of a single splitter, we consider the configuration 1PARA represented in Fig. 4(a) as the simplest, nontrivial LANER. The gains are oriented (in all the examples) according to the arrows depicted in the figure; i.e., the propagation gain along the arrow in a link j is G_j and G_j^* in the opposite direction. The propagation matrix is given in the appendix. In the case of two splitters, we consider the 2PARA and 2PERP configurations as depicted in Figs. 4(b) and 4(c), respectively. Their matrices are also reported in the appendix.

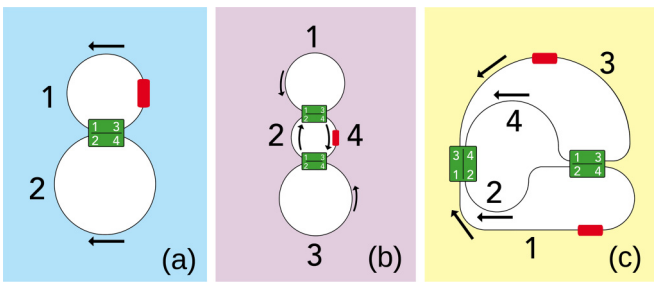

FIG. 4. LANER examples: (a) 1PARA, (b) 2PARA, and (c) 2PERP. The arrows indicate the (arbitrarily chosen) reference propagation directions. Red blocks depict possible position choices for the active gains.

We mention that for the simple configurations such as the 1PARA and 2PARA, the representative graphs are disjoint [15], indicating that two sets of independent propagations are possible in such LANERs. Such a feature in terms of ray dynamics can be interpreted as the independence of the two correspondent Euler paths [27] in the graph.

Let us illustrate in Fig. 5 the spectral and emission features for the three configurations. We first show the onset of the laser action by computing the poles $s_n = \mu_n + ik_n$ numerically from Eq. (12) and plotting them in the complex plane for increasing gain values [see Figs. 5(b), 5(d) and 5(f)]. In all cases, above a critical value, a set of resonances cross the real axis and the associated modes grow with rate $\mu_n > 0$ and start to lase. Since we assumed an infinite gain bandwidth, the dynamics will involve an infinite number of unstable modes above threshold (in practice, it will be very high dimensional, with order of 10^5 or more modes [15]). Also, we checked that the integrated density of states, namely the number of modes below k grows on average linearly, as expected from the Weyl law for one-dimensional structure [18].

What is experimentally accessible is the beating spectrum of the field intensity measured at the detection point x_0 along the chosen direction, i.e., the modulus of the Fourier transform of the modulus of the field F,

$$|F(x_0)|^2 = |\Sigma_n F_n e^{-ik_n x_0}|^2 = \Sigma_{n,m} F_n F_m^* e^{-i(k_n - k_m)x_0}, \quad (13)$$

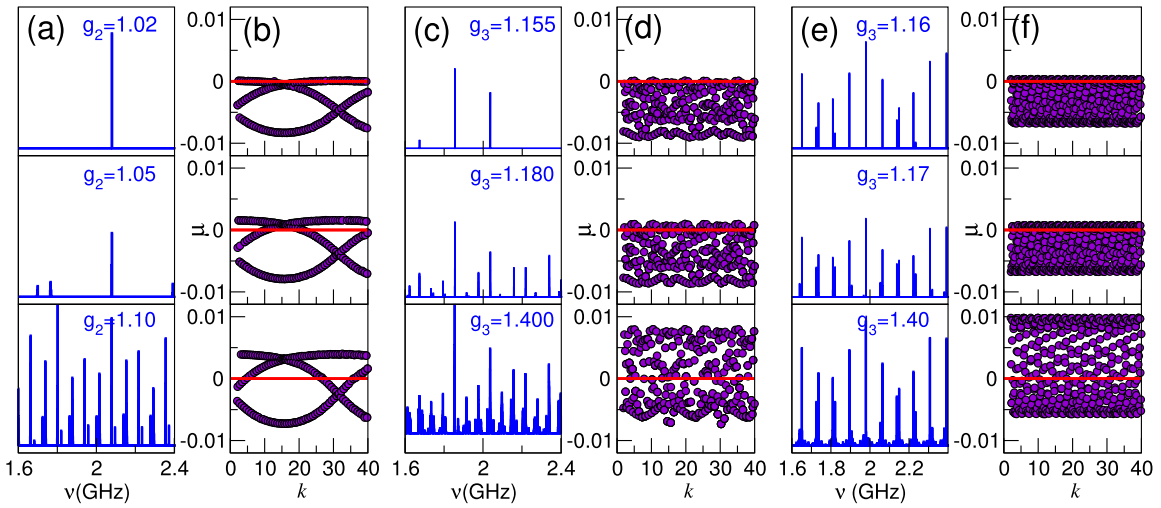

FIG. 5. (Numerics) Threshold behavior of various LANER systems upon increasing gain on one link. Results for 1PARA [(a), (b)], 2PARA [(c), (d)], and 2PERP [(e), (f)]. Panels (a), (c), and (e) are the beating spectra (in arbitrary units) computed as described in the text; panels (b), (d), and (f) are poles in the complex plane. The chosen lengths are $L_1 = 9.16$ m, $L_2 = 18.12$ m (1PARA) and $L_1 = 9.16$ m, $L_2 = 18.12$ m, $L_3 = 5.24$ m, $L_4 = 10.0$ m (2PARA, 2PERP); the loss factors are $g_j = 0.9$ on all the links except the one specified in the figures. The spectra are computed considering roughly 10^3–10^4 poles in each case.

showing peaks at all the possible differences (within the available detection bandwidth) of the optical modes involved. Thus, for a given set of M values of the wave numbers k_n, we compute all the differences $k_n - k_m$ belonging to a given interval $(0, \beta)$, with β being an assigned bandwidth. Such beatings are evaluated for the lasing modes (those with $\mu_n > 0$) and their distribution is plotted [see Figs. 5(a), 5(c) and 5(e)]. The result represents a qualitative estimation, showing a structure that can be directly compared with the experiment.

V. THE LANER AS A LATTICE

An important case to consider is when the links are all multiples of the same length L_0, i.e., the LANER is a lattice and L_0 is the lattice periodicity:

$$L_j = n_j L_0, \tag{14}$$

with $\{n_j\}$ being a set of positive integers. Such a circumstance is intentionally avoided in the quantum graphs literature as it may lead to dynamical quasiperiodicity that hinders the observation of universal spectral features [18] but it is very instructive to gain insight in the spectral structure.

According to Eq. (14), the gain terms turn to be invariant under the transformation $s \to s + iK_0$, where $K_0 = 2\pi/L_0$. The spectrum is therefore periodic along the wave-vector (imaginary) axis and the period K_0 is the free spectral range (FSR; see, e.g., Ref. [12]) of the cavity: The above result amounts to identify the FSR with the first Brillouin zone in solid-state physics (see, e.g., Ref. [28]). In particular, one can consider the first zone as $[-\pi/L_0, \pi/L_0)$ and, since if s is a solution s^* is a solution as well, it follows that the independent solutions are only those in $[0, \pi/L_0)$.

Another remarkable feature is that in this case the poles can be evaluated as zeros of a polynomial and can be thus enumerated exactly. To see this, let us introduce the complex variable $e^{-sL_0} = z$ and define

$$Q(z, z^*) = \det(N - I)\,. \tag{15}$$

In the case of symmetric scalar gains, by inspection of Q one can find that all its terms are of the form

$$a_j z^m (z^*)^l + a_j^* z^l (z^*)^m, \tag{16}$$

where the coefficients a are products of the g's. Indeed, since in our case P is Hermitian and S is real and symmetric, it holds that

$$\begin{aligned} Q^* &= \det(P^* S^* - I) \\ &= \det((SP)^T - I) = \det(SP - I) = Q\,. \end{aligned} \tag{17}$$

Q is thus a real polynomial, with a degree $D = \sum_l n_l$ both in z and z^*, and admits D solutions in the Brillouin (half) zone. The full solution for the poles s is obtained by periodic extension taking all branches of the logarithm function with the appropriate periodicity.

We notice that in general the characteristic equation

$$\det(N(G, G^*) - I) = C(G, G^*) = 0, \tag{18}$$

where for brevity $\{G, G^*\}$ denotes the arrays of the G_j, G_j^*, must admit the same set of solutions not only by replacing $G_j \leftrightarrow G_j^*$ for all j's (to invert all the propagation direction in the links) but also in the case of the more general symmetry

$$G_j \leftrightarrow G_j^*,\ j \in H, \tag{19}$$

where H is an arbitrary subset of the links index set. As said, such a property is a direct consequence of the possibility to choose arbitrarily the propagation direction in every link.

Besides, it is always possible to write the propagation matrix as

$$P(G, G^*) = T_1(G, G^*) + T_2(G, G^*), \tag{20}$$

where T_1 (respectively, T_2) is a lower (upper) triangular matrix and, with a proper choice of the orientation in the links, we

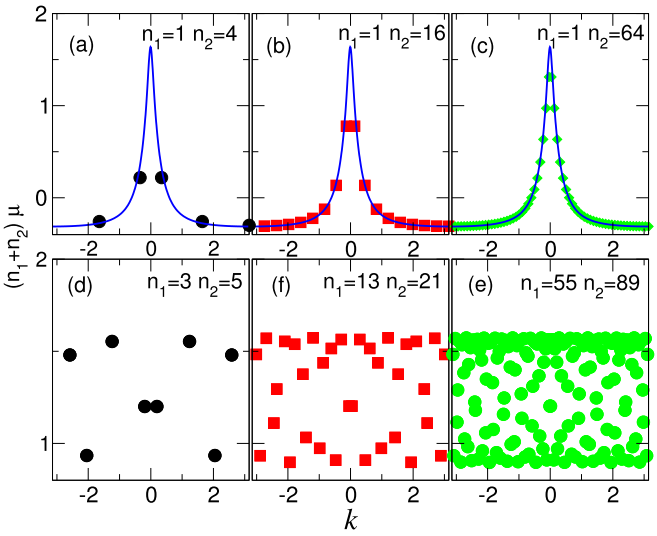

FIG. 6. The poles in the complex plane for the 1PARA configuration with lengths having rational rations; see Eq. (23) and text. Only the data in the range $|k| < \pi/L_0$ are reported (corresponding to first Brillouin zone); the gains are $g_1 = 1.3$, $g_2 = 0.7$. [(a)–(c)] Case $n_2 = Nn_1$, solid blue line is the analytical curve, Eq. (26); [(d)–(e)] n_1 and n_2 are successive values of the Fibonacci series. For comparison, the real parts have been multiplied by the total length $(n_1 + n_2)$.

can order the gains in such a way that, e.g., all and only the G's (respectively, G^*'s) are T_1 (T_2) elements. Finally, using $P = P^\dagger$, it follows that

$$P(G, G^*) = T(G) + T(G)^\dagger, \tag{21}$$

where $T = T_1$. The characteristic equation thus can be solved by considering

$$C(G, G) = 0, \tag{22}$$

together with the symmetry $G_j \leftrightarrow G_j^*, \forall j$ (if G_j is a solution G_j^* is a solution as well).

As an example, we discuss the 1PARA spectrum in the lattice configuration. We first set

$$L_1 = n_1 L_0,\ L_2 = n_2 L_0; \tag{23}$$

to find the poles of the characteristic equation is sufficient to solve

$$1 + g_1 g_2 z^{n_1+n_2} - \frac{1}{\sqrt{2}}(g_1 z^{n_1} + g_2 z^{n_2}) = 0, \tag{24}$$

where $z = e^{-sL_0}$, given the spectrum symmetry discussed above.

For illustration, let us first consider the case $n_2 = Nn_1$, where now $z = e^{-sn_1 L_0}$, yielding $N + 1$ solutions of Eq. (24) for z. Then, for each of them we need to solve an n_1-order equation for the s, obtaining n_1 poles with the same real part. Therefore, the spectrum displays a further symmetry, splitting in n_1 profiles (i.e., the Brillouin zone), each containing $N + 1$ poles.

As seen in the Figs. 6(a)–6(c), for increasing N the poles distribute along a well-defined curve after a suitable rescaling of the real part. This can be demonstrated analytically looking for solutions of the type

$$z = e^{-(\mu+ik)L_0} = e^{-(y(x)/N+ix)L_0}, \tag{25}$$

where x, y are independent of N for $N \gg 1$. Substituting in the polynomial equation, we obtain

$$y(x) = \log\left|\left(g_1 e^{-ix} - \frac{1}{\sqrt{2}}\right)g_2\right| - \log\left|1 - \frac{1}{\sqrt{2}} g_1 e^{-ix}\right|, \tag{26}$$

which is depicted as a solid line in the figure, showing a very good agreement with the numerical solutions.

Another interesting example is the case in which the integers n_1 and n_2 are pairs of consecutive terms in the Fibonacci series so that the ratio of the two physical lengths L_2/L_1 approaches the golden ratio $(\sqrt{5} + 1)/2$ for increasingly large n_1 and n_2. Some of the first steps of the construction are given in Figs. 6(d)–6(e) that allows us to appreciate the structure of the spectrum. It should be noticed that the poles are confined in a horizontal strip in the complex plane, meaning that the growth and decay rates are bounded.

As an additional remark, note the qualitative similarity of the spectra obtained by rational approximation with the numerical solution reported in Fig. 5(b), originating from the choice $L_2 \approx 2L_1$. This confirms that the procedure illustrated in this section can be useful to understand the spectral structure.

To conclude this section, we remark that the lattice approach can be an effective description of real setups. Indeed, when using arbitrary length fibers and splitters, the LANER can be approximated by a sequence of lattices with increasingly smaller periodicity L_0.; e.g., $L_0 \to 10^{-r} L_0$, leading to $n_j \to 10^r n_j$. As a consequence, the link length is described by an increasing number of digits and the spectrum remains almost the same upon rescaling of the frequency axis (by a factor $\approx 10^r$). This approach can be thus considered as an increasingly accurate rational approximation of the spectrum. In a physical system, the ultimate limit for L_0 would be represented by the field wavelength; in practice, many effects may affect the observable FSR.

VI. EXPERIMENT

A. Experimental setup

In this section, we present the main phenomenology found in the experimental realizations of the configurations outlined in Fig. 4, focusing on the laser emission and the basic features of the spectrum and leaving more detailed and specific investigations to future studies. Indeed, besides the features of a laser process that can be evidenced already in the dc total intensity, a complicated structure of the emission spectrum of a LANER is expected as, e.g., gain is varied.

As discussed in Sec. II, a LANER can be physically realized in many ways depending on the components chosen. For instance, a different splitting ratio of the 2×2 unitary splitters considered before can strongly influence the results obtained in the same topology already in the simplest configurations.

In the present work, we focus on experimental setups characterized by the choices: The physical network is build

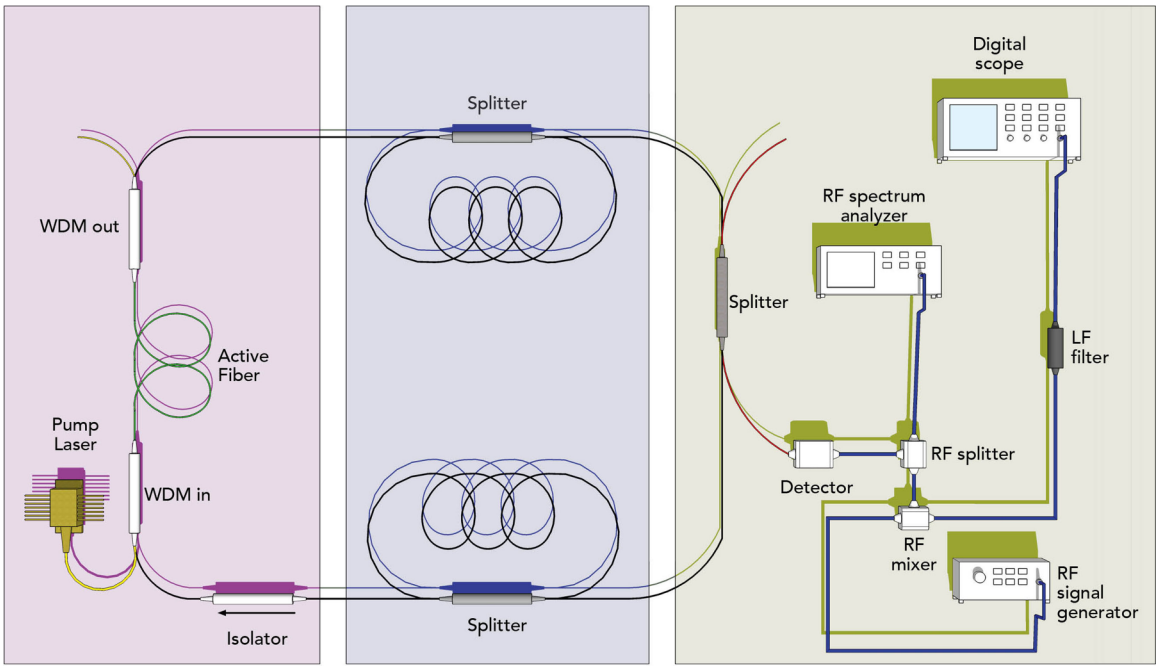

FIG. 7. Block setup for the case of Fig. 4(b) (2PARA). Left: (Oriented) active section composed of a 980-nm pumped, Er^{3+} fiber, WDMs combining and separating pump and 1.55-μm signals and an optical isolator. Center: The rest of the system. Right: The frequency and time-domain detection and acquisition section.

using single-mode optical fibers and standard, 2×2 lossless, reciprocal, and matched optical splitters. The 50 : 50 splitting ratio has been used in the all configurations here considered. An example of an experimental setup organized in a block structure is outlined in Fig. 7.

The gain in the active links is provided by ≈1.5-m erbium-doped optical fiber(s), pumped by 980-nm power laser(s). In the gain section(s), input and output wavelength demultiplexers (WDMs) are used to couple and decouple the pump beam to and from the 1550-nm signal beam. The unused output port of the WDM-OUT can be used to monitor the amount of pump power not absorbed by the system. The active links are directed; i.e., optical isolators assure the unidirectional propagation of the signal beam. This represents a relevant simplification in the expected experimental effects, since possible spatial effects in the active medium (such as spatial hole burning due to the interference between the two counterpropagating fields) are avoided. The currents of the pump lasers represent the main control parameters of our setup, as they are directly related to the coherent amplification in the active links: An arbitrary number of them can be active simultaneously and independently. A single-gain, directed setup for an active link is depicted in the left part of Fig. 7.

The detection is performed by inserting in a link a 2×2 optical coupler with ratio of 50 : 50. The split field intensity is collected in the proper direction either with high-bandwidth (8 GHz) or low-bandwidth (150 MHz), high-sensitivity photodetectors. The detector current is then sent to a radio-frequency spectrum analyzer and/or a fast digital oscilloscope. A detection and measuring section is illustrated in the right part of Fig. 7.

B. Experimental results

The first experimental configurations investigated are depicted in Fig. 8. A main ring is built including the active fiber, an optical isolator, and three 50 : 50 optical splitters; one of them is devoted to bring out the field for the detection. The total length of the ring is measured pumping the active fiber in order to have a laser emission. The measured intensity spectrum, characterized by equally spaced peaks is typical of a ring laser (see, e.g., Ref. [12]) and allows us to estimate the cavity length by measuring the peak frequency separation. With the same method, by properly replacing the fiber links, it is possible to measure the lengths of the other rings. In the configuration depicted in the figure, some additional optical splitters have been inserted (such as those in the upper and lower rings) to gain flexibility in the reorganization of the links at the expenses of an higher level of losses in the cavity. In particular, we can switch from the 1PARA to the 2PARA configuration by inserting the upper fiber only (the part in the dashed lines box), while maintaining all the features (e.g., lengths) of the rest of the physical network. Notably, in this case the level of losses will decrease because the upper splitter will not drain power: We therefore expect at least a different value for the threshold current in the two configurations.

As a first result, we present in Fig. 9 the total emission curve as a function of the pump laser current for the 1PARA configuration. This is obtained by a direct measurement of the emitted intensity with a 1.55-μm optical power meter (black curves), and simultaneously monitoring the fraction of the 980-nm pump laser intensity (red curve) exiting from the unused output port of the WDM-OUT (see also Fig. 7). A clear evidence of a laser emission is obtained, with the typical

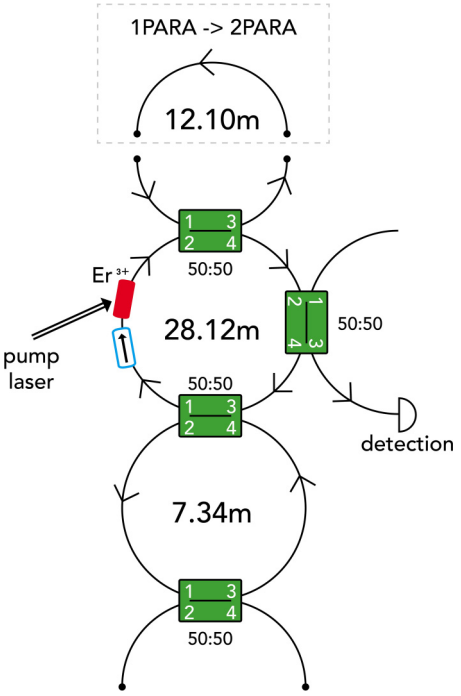

FIG. 8. Experimental setup for the 1PARA and 2PARA configurations. The unconnected ports of the splitters allow us to expand the LANER without modifications to the existing parts (see the top ring), at the expenses of an higher amount of losses in the simpler arrangements.

intensity-versus-pump behavior displaying a threshold point at $I = 43.1$ mA.

As seen in the figure, the change in the slope (corner) of the red curve indicates a strong change in the energy absorbed

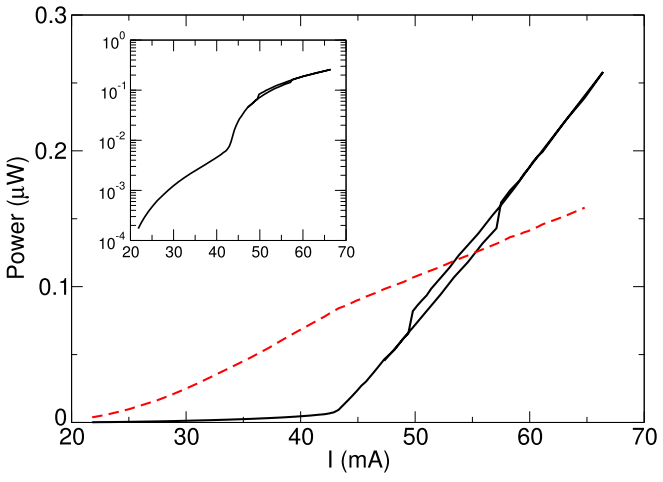

FIG. 9. Measurements of the LANER emitter power as a function of the laser pump current (black) for the 1PARA configuration. An hysteresis cycle is visible for intermediate pumping power. Inset: the same curve in semilog scale showing clearly the lasing transition. Red curve: laser pump power measured at the unused port of the WDM-out (see Fig. 7); the curve has been rescaled for comparison. The slope change indicates the LANER threshold at $I = 43.1$ mA as well.

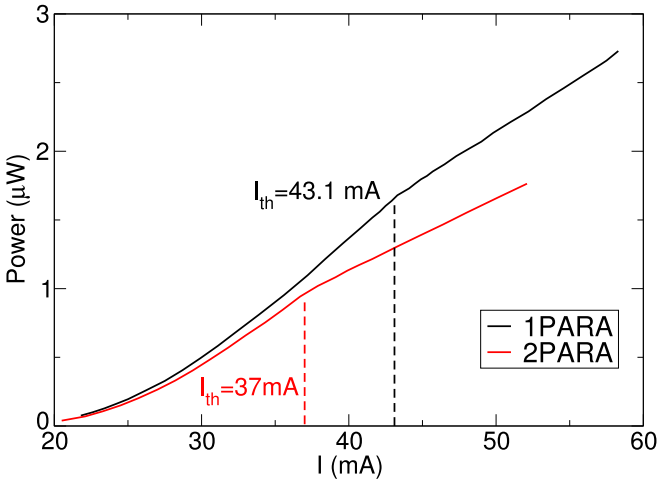

FIG. 10. Measurement of the laser pump power detected at the unused port of the WDM-out (see Fig. 7) for the 1PARA and 2PARA configurations. The corner points indicating the thresholds are marked.

by the erbium active medium as the lasing process starts. This method allows an easier estimation of the threshold since the monitoring does not need to reconfigure the detection setup. As an example, we report in Fig. 10 the threshold estimation in the 1PARA and 2PARA setups performed in this way.

We also observe that a different level of emission, resulting in an hysteresis cycle when increasing and decreasing the pump laser current is found at intermediate level of pumping (see Fig. 9). Such a phenomenon is expected when nonlinear effects related to far-from-threshold pumpings enter into play and this will be the object of further investigations.

The dynamics in erbium-doped fiber laser is commonly expected [29] to belong to the class-B lasers [30]. In such a class, a peculiar feature of the laser dynamics is the relaxation toward stationary, stable lasing states through damped oscillations. Such transient phenomenon, named relaxation oscillations (RO) (see, e.g., Ref. [31]) can be observed in the presence of noise as well as a sustained peak in the laser intensity power spectrum. A typical feature of RO is the square-root scaling of their frequency with the normalized laser pump current $(I - I_{\rm th})/I_{\rm th}$, where $I_{\rm th}$ is the laser pump current threshold.

We report in Fig. 11 the direct measurement of the frequency of RO both in the 1PARA and 2PARA configurations. The curves follow the predicted scaling with the pump, thus confirming the laser nature of the LANER emission. It is interesting to note that a strong separation is observed between the dynamical oscillation frequencies, related to the field propagation delays on the MHz scales, and the natural frequency of the RO the kHz scales, which is instead pump dependent.

Most of the dynamical features of the LANER emission can be studied in the spectrum of the emitted intensity, as it can be compared with the findings of the linear theory. It is worth remembering, however, that the detected signal spectrum shows the beatings of the optical modes involved which are estimated by the theory.

In Fig. 12, we show the power spectrum of the emitted intensity in the 1PARA configuration for increasing values of

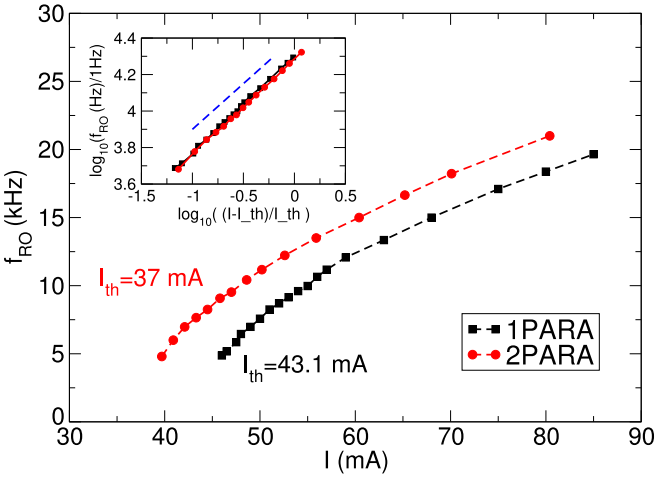

FIG. 11. Measurements of the relaxation oscillations frequency for the 1PARA and 2PARA configurations as a function of the pump laser current. Inset: rescaled curves for the two configurations (see text). The dashed line is a power law with exponent 1/2.

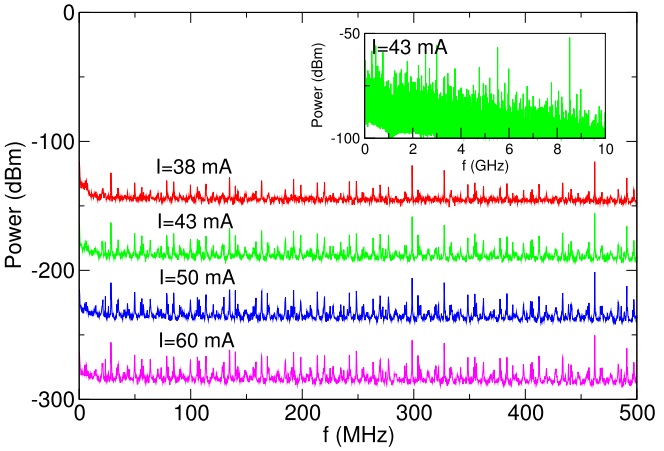

FIG. 13. Experimental power spectra of the LANER emitted intensity in the 2PARA configuration for increasing values of the pump laser current. The threshold is $I_{\rm th} = 37$ mA. Each spectrum is shifted vertically by 50 dB from the previous one. The inset is a larger bandwidth spectrum at $I = 43$ mA.

the pump laser current. Below the threshold value (at about $I = 43.1$ mA as said), no emission is obtained (see the first top spectrum); increasing the pump, the emission starts and many peaks appear, distributed in an irregular but apparently close to a periodic sequence. As shown in the figure (see also the inset), increasing the pump apparently does not produce relevant changes in the beating spectrum, apart from a general increase of the peak height. In particular, the smaller peaks could be generated by the beatings between higher harmonics due to nonlinear effects.

In Fig. 13, we report the same type of measurement for the 2PARA configuration realized by adding the top fiber link as shown in Fig. 8. The approximate periodicity of the spectrum is quickly lost for more complicated configurations (see also the inset), at least in the available measurement bandwidth window.

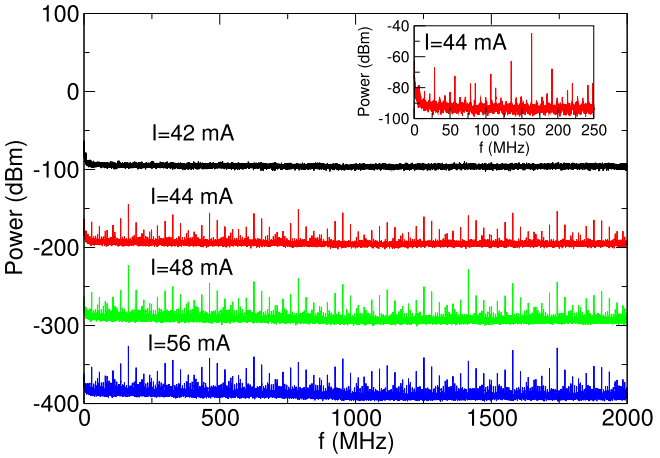

FIG. 12. Experimental power spectra of the LANER emitted intensity in the 1PARA configuration for increasing values of the pump laser current. The threshold is $I_{\rm th} = 43.1$ mA. Each spectrum is shifted vertically by 100 dB from the previous one. The inset is an enlargement of the spectrum at $I = 44$ mA.

As a final example, we consider the 2PERP configuration sketched in Fig. 14. A peculiar feature of this setup is the presence of two active links, each realized as in the left block of Fig. 7. Notably, while in the previous 1PARA and 2PARA setups the optical isolator determined the unidirectional propagation in all the system, this does not occur in the 2PERP even using two of them. In particular, as can be seen in Fig. 14, the (forced) unidirectional propagation in the links 1 and 4 does not *a priori* lead to same behavior in the links 2 and 3; therefore, both sides of the detection splitter can be used to simultaneously measure the fields in the two directions.

In the present work, we limit ourselves to present the effect of the two combined gains as shown in Fig. 15, in a regime where both the pumped fibers are acting as coherent amplifiers (i.e., the corresponding pump laser currents are

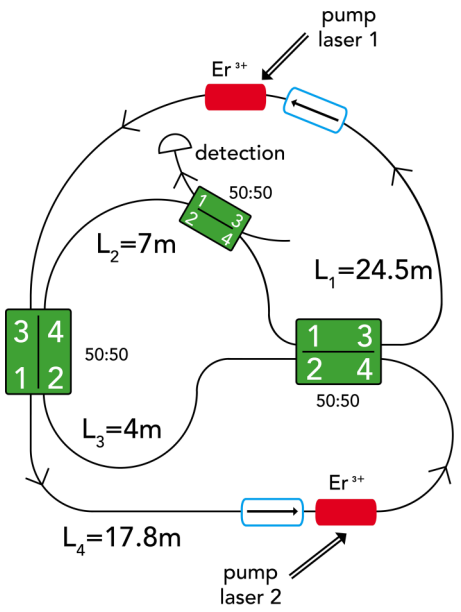

FIG. 14. Experimental setup for the 2PERP configuration.

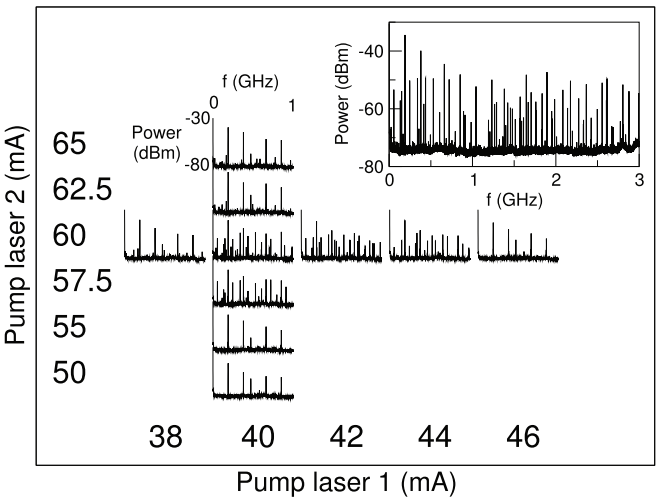

FIG. 15. Experimental power spectra for the 2PERP configuration when scanning the two pump laser currents. The inset shows a larger bandwidth spectrum for $I_1 = 40$ mA, $I_2 = 60$ mA.

large enough). As shown in the figure, a complicated situation occurs, with structured spectra with many peaks found in the two-dimensional parameter space of the gains. Multistabilities in the emission are also possible, as a consequence of the interplay of the involved fields.

All the reported phenomenology measured in the three configurations can be compared with those evaluated by computing the linear spectra in Fig. 5, showing a good qualitative agreement.

VII. CONCLUSIONS

The LANER represents an optical scheme generalizing the standard laser setups, both in the geometry of the cavity and in the number of active media providing coherent amplification. In this work, we have described in details the main ingredients of the system, remarking on the generality of the approach potentially capable of employing a large variety of components to obtain increasingly complicated configurations. The LANER can also represent a powerful and flexible experimental framework for the investigation of the dynamics on a physical network, where all the control parameters and the variables (related to the involved optical fields) can be easily measured.

In a theoretical approach, the LANER is described by a general propagation matrix containing the connections (topology) and the lengths and gains (metrics). A global scattering matrix, containing the transfer properties of the optical couplers connecting the links, provides the suitable boundary conditions for the fields. The problem defined by Eq. (12) for the LANER matrix allows the determination of the poles for the wave solutions of the system representing the generalization of the corresponding problem for the standard laser. The structure of the solutions resembles that found for highly multimode laser systems; however, a LANER could be much more complicated because of the freedom in its topology (i.e., the geometry of the connections).

Besides the details of the theoretical description, we have discussed some specific limit cases of particular interest as they relate to well-known frameworks: the Hamiltonian (gain- and lossless cavity) and lattice (all links multiples of the same length) setups. They both show the potentiality of the LANER to experimentally realize such difficult schemes. Furthermore, the close connection with the graph theory is suggested with a general method to represent a LANER as a directed graph, determining easily the adjacency matrix of the latter. In this way, an even closer connection with the quantum chaos topics and the problem of amplification and diffusion on a graph has been established.

To provide examples of the approach, we have studied some simple configurations that can be realized with few couplers, showing the corresponding matrices and numerical solutions of the characteristic problem with the determination of the poles.

From an experimental point of view, a general discussion of the possible implementations has been provided, suggesting that a completely new avenue of studies can be initiated. Furthermore, we have presented the specific phenomenology of the experimental realizations of the simpler configurations studied in the theory, giving evidence of the onset of the laser emission above a critical pumping of the active media. We have also reported measurements of the spectra of the emitted intensity where the beatings of the involved modes depict a complicated scenario. As shown by our experiments, the setup is more suited to study small networks. However, possible implementation with scalable integrated optics devices can be envisaged to easily realize networks of hundreds to thousands elements.

To conclude, we have characterized the LANER as an optical scheme with laser action and a fully controllable topological disorder induced by the link connections. Since multiple and independent gain sections can be used as well, the LANER would allow new investigations, ranging from dynamics on physical networks of increasing size to the effect of the cavity topology on the laser emission. We finally remark that the identifications of the key points leading to general results will represent a major challenge of this research.

ACKNOWLEDGMENT

We thank F. Cherubini for help in the drawings. Authors are listed in alphabetical order.

APPENDIX: LANER EXAMPLES MATRICES

The 1PARA propagation matrix is

$$P = \begin{pmatrix} 0 & 0 & G_1 & 0 \\ 0 & 0 & 0 & G_2 \\ G_1^* & 0 & 0 & 0 \\ 0 & G_2^* & 0 & 0 \end{pmatrix} \tag{A1}$$

and the network matrix is

$$N = PS = \frac{1}{\sqrt{2}} \begin{pmatrix} G_1 & -G_1 & 0 & 0 \\ G_2 & G_2 & 0 & 0 \\ 0 & 0 & G_1^* & G_1^* \\ 0 & 0 & -G_2^* & G_2^* \end{pmatrix}. \tag{A2}$$

In this case, Eq. (12) factorizes as

$$\left[1+G_1^*G_2^*-\frac{1}{\sqrt{2}}(G_1^*+G_2^*)\right]\left[1+G_1G_2-\frac{1}{\sqrt{2}}(G_1+G_2)\right]=0\,. \tag{A3}$$

The 2PARA propagation matrix is

$$P=\begin{pmatrix} 0 & 0 & G_1 & 0 & 0 & 0 & 0 & 0\\ 0 & 0 & 0 & 0 & G_2 & 0 & 0 & 0\\ G_1^* & 0 & 0 & 0 & 0 & 0 & 0 & 0\\ 0 & 0 & 0 & 0 & 0 & 0 & G_3^* & 0\\ 0 & G_2^* & 0 & 0 & 0 & 0 & 0 & 0\\ 0 & 0 & 0 & 0 & 0 & 0 & 0 & G_4^*\\ 0 & 0 & 0 & G_3 & 0 & 0 & 0 & 0\\ 0 & 0 & 0 & 0 & 0 & G_4 & 0 & 0 \end{pmatrix} \tag{A4}$$

and the network matrix is

$$N=\frac{1}{\sqrt{2}}\begin{pmatrix} G_1 & -G_1 & 0 & 0 & 0 & 0 & 0 & 0\\ 0 & 0 & 0 & 0 & 0 & 0 & G_2 & G_2\\ 0 & 0 & G_1^* & G_1^* & 0 & 0 & 0 & 0\\ 0 & 0 & 0 & 0 & G_3^* & -G_3^* & 0 & 0\\ 0 & 0 & -G_2^* & G_2^* & 0 & 0 & 0 & 0\\ 0 & 0 & 0 & 0 & G_4^* & G_4^* & 0 & 0\\ G_3 & G_3 & 0 & 0 & 0 & 0 & 0 & 0\\ 0 & 0 & 0 & 0 & 0 & 0 & -G_4 & G_4 \end{pmatrix}.$$

The 2PERP propagation matrix is

$$P=\begin{pmatrix} 0 & 0 & 0 & 0 & 0 & 0 & 0 & G_1\\ 0 & 0 & 0 & 0 & 0 & G_2 & 0 & 0\\ 0 & 0 & 0 & 0 & 0 & 0 & G_3 & 0\\ 0 & 0 & 0 & 0 & G_4 & 0 & 0 & 0\\ 0 & 0 & 0 & G_4^* & 0 & 0 & 0 & 0\\ 0 & G_2^* & 0 & 0 & 0 & 0 & 0 & 0\\ 0 & 0 & G_3^* & 0 & 0 & 0 & 0 & 0\\ G_1^* & 0 & 0 & 0 & 0 & 0 & 0 & 0 \end{pmatrix} \tag{A5}$$

and the network matrix is

$$N=\frac{1}{\sqrt{2}}\begin{pmatrix} 0 & 0 & 0 & 0 & G_1 & G_1 & 0 & 0\\ 0 & 0 & 0 & 0 & 0 & 0 & -G_2 & G_2\\ 0 & 0 & 0 & 0 & G_3 & -G_3 & 0 & 0\\ 0 & 0 & 0 & 0 & 0 & 0 & G_4 & G_4\\ G_4^* & G_4^* & 0 & 0 & 0 & 0 & 0 & 0\\ 0 & 0 & -G_2^* & G_2^* & 0 & 0 & 0 & 0\\ G_3^* & -G_3^* & 0 & 0 & 0 & 0 & 0 & 0\\ 0 & 0 & G_1^* & G_1^* & 0 & 0 & 0 & 0 \end{pmatrix}.$$

[1] S. Boccaletti, V. Latora, Y. Moreno, M. Chavez, and D.-U. Hwang, Phys. Rep. **424**, 175 (2006).

[2] M. A. Porter and J. P. Gleeson, in *Dynamical Systems on Networks: A Tutorial*, Frontiers in Applied Dynamical Systems: Reviews and Tutorials (Springer, Berlin, 2016).

[3] M. Rohden, A. Sorge, M. Timme, and D. Witthaut, Phys. Rev. Lett. **109**, 064101 (2012).

[4] I. Belykh, M. Hasler, M. Lauret, and H. Nijmeijer, Int. J. Bif. Chaos **15**, 3423 (2005).

[5] M. Barthelemy, *Morphogenesis of Spatial Networks* (Springer, Berlin, 2018).

[6] R. Burioni, D. Cassi, M. Rasetti, P. Sodano, and A. Vezzani, J. Phys. B **34**, 4697 (2001).

[7] H. Pichler, T. Ramos, A. J. Daley, and P. Zoller, Phys. Rev. A **91**, 042116 (2015).

[8] S. Gnutzmann, U. Smilansky, and S. Derevyanko, Phys. Rev. A **83**, 033831 (2011).

[9] F. Perakis, M. Mattheakis, and G. Tsironis, J. Opt. **16**, 102003 (2014).

[10] B. Bellazzini and M. Mintchev, J. Phys. A: Math. Gen. **39**, 11101 (2006).

[11] S. Gnutzmann and U. Smilansky, Philos. Trans. A Math. Phys. Eng. Sci. **372**, 20130264 (2014).

[12] P. W. Milonni and J. H. Eberly, *Laser Physics.* (John Wiley & Sons, New York, 2010).

[13] H. Cao, Waves Random Media **13**, 1 (2003).

[14] D. S. Wiersma, Nat. Phys. **4**, 359 (2008).
[15] S. Lepri, C. Trono, and G. Giacomelli, Phys. Rev. Lett. **118**, 123901 (2017).
[16] D. M. Pozar, *Microwave Engineering* (John Wiley & Sons, New York, 2011).
[17] P. Kuchment, Waves Random Media **14**, S107 (2004).
[18] T. Kottos and U. Smilansky, Ann. Phys. **274**, 76 (1999).
[19] T. Kottos and U. Smilansky, J. Phys. A **36**, 3501 (2003).
[20] F. Barra and P. Gaspard, Phys. Rev. E **65**, 016205 (2001).
[21] O. Hul, S. Bauch, P. Pakoński, N. Savytskyy, K. Życzkowski, and L. Sirko, Phys. Rev. E **69**, 056205 (2004).
[22] F. Barra and P. Gaspard, Phys. Rev. E **63**, 066215 (2001).
[23] E. Ignesti, F. Tommasi, L. Fini, S. Lepri, V. Radhalakshmi, D. Wiersma, and S. Cavalieri, Phys. Rev. A **88**, 033820 (2013).
[24] R. Uppu and S. Mujumdar, Phys. Rev. A **90**, 025801 (2014).
[25] B. C. Lima, A. S. Gomes, P. I. Pincheira, A. L. Moura, M. Gagné, E. P. Raposo, C. B. de Araújo, and R. Kashyap, J. Opt. Soc. Am. B **34**, 293 (2017).
[26] R. Burioni and D. Cassi, J. Phys. A **38**, R45 (2005).
[27] G. Chartrand, *Introductory Graph Theory* (Dover, New York, 1985).
[28] N. W. Ashcroft and N. D. Mermin, *Introduction to Solid State Physics* (Saunders, Philadelphia, 1976).
[29] A. Bellemare, Prog. Quantum Electron. **27**, 211 (2003).
[30] F. T. Arecchi, *Instabilities and Chaos in Quantum Optics* (Springer, Berlin, 1987).
[31] H. Haken, *Light: Laser light dynamics* (North-Holland Physics, Amsterdam, 1985), Vol. 2.